Brain DNA methylomic analysis of frontotemporal lobar degeneration reveals *OTUD4* and *CEBPZ* in shared dysregulated signatures across pathological subtypes

Katherine Fodder[1,2], Megha Murthy[1,3], Patrizia Rizzu[4], Christina E. Toomey[1,3,5], Rahat Hasan[6], Jack Humphrey[6], Towfique Raj[6], Katie Lunnon[7], Jonathan Mill[7], Peter Heutink[4], Tammaryn Lashley[1,2], Conceição Bettencourt[1,2,*]

1. Queen Square Brain Bank for Neurological Disorders, UCL Queen Square Institute of Neurology, London, UK.
2. Department of Neurodegenerative Disease, UCL Queen Square Institute of Neurology, London, UK.
3. Department of Clinical and Movement Neurosciences, UCL Queen Square Institute of Neurology, London, UK.
4. German Center for Neurodegenerative Diseases (DZNE), Tübingen, Germany.
5. The Francis Crick Institute, London, UK.
6. Nash Family Department of Neuroscience & Friedman Brain Institute, Icahn School of Medicine at Mount Sinai, New York, NY, USA.
7. Department of Clinical and Biomedical Sciences, Faculty of Health and Life Sciences, University of Exeter, Exeter, UK.

***Corresponding Author:**

Conceição Bettencourt, PhD

Department of Neurodegenerative Disease

UCL Queen Square Institute of Neurology

Queen Square Brain Bank for Neurological Disorders

1 Wakefield Street

London WC1N 1PJ

United Kingdom

Email c.bettencourt@ucl.ac.uk

ABSTRACT

Frontotemporal lobar degeneration (FTLD) is an umbrella term describing the neuropathology of a clinically, genetically and pathologically heterogeneous group of diseases, including frontotemporal dementia (FTD) and progressive supranuclear palsy (PSP). Among the major FTLD pathological subgroups, FTLD with TDP-43 positive inclusions (FTLD-TDP) and FTLD with tau positive inclusions (FTLD-tau) are the most common, representing about 90% of the cases. Although alterations in DNA methylation have been consistently associated with neurodegenerative diseases, namely Alzheimer's disease, little is known for FTLD and its heterogeneous subgroups and subtypes. The main goal of this study was to investigate DNA methylation variation in FTLD-TDP and FTLD-tau. We used frontal cortex genome-wide DNA methylation profiles from three FTLD cohorts (228 individuals), generated using the Illumina 450K or EPIC arrays. We performed epigenome-wide association studies (EWAS) for each cohort followed by meta-analysis to identify shared differential methylated loci across FTLD subgroups/subtypes. Additionally, we used weighted gene correlation network analysis to identify co-methylation signatures associated with FTLD and other disease-related traits. Wherever possible, we also incorporated relevant gene/protein expression data. The EWAS meta-analysis revealed four differentially methylated loci in FTLD, some of which showed altered gene and protein expression in FTLD. Two of the meta-analysis hits, *OTUD4* and *CEBPZ*, were found to be co-methylated within signatures strongly associated with FTLD. These signatures were enriched for genes implicated in the ubiquitin system, RNA/stress granule formation and glutamatergic synaptic signalling. Altogether, our findings identified novel FTLD-associated loci, and support a role for DNA methylation as a mechanism involved in the dysregulation of biological processes relevant to FTLD, highlighting novel potential avenues for therapeutic development.

Keywords: DNA methylation; frontotemporal dementia; progressive supranuclear palsy; human brain tissue; EWAS; co-methylation

INTRODUCTION

Frontotemporal lobar degeneration (FTLD) is an umbrella term describing the neuropathology of a group of neurodegenerative disorders, which all have in common the selective degeneration of the frontal and temporal lobes of the brain. These disorders are clinically, pathologically and genetically heterogeneous. Clinically, patients with FTLD frequently present with frontotemporal dementia (FTD), which is the second most common form of early onset dementia, and is often associated with behavioural and language changes. A fraction of patients may present with or develop parkinsonism as part of their disease, including those with progressive supranuclear palsy (PSP), and frontotemporal dementia and parkinsonism linked to chromosome 17 (FTDP-17). An overlap with amyotrophic lateral sclerosis/motor neuron disease (ALS/MND) is also observed in a proportion of patients with FTLD, highlighting a spectrum of clinical phenotypes that relate to shared neuropathologic features[1,2].

A considerable number of FTLD cases report a positive family history (30-50%), and the majority of familial cases can be explained by mutations in three genes, namely chromosome 9 open reading frame 72 (*C9orf72*), progranulin (*GRN*), and microtubule-associated protein tau (*MAPT*). Apart from those cases in which a genetic mutation has been identified, neuropathological assessment is essential to confirm the disease entity underlying FTLD. The neuropathological classification of FTLDs, based on the presence/absence of specific proteinaceous inclusions, recognizes five major subgroups. FTLD with 43 kDa transactive response DNA-binding protein (TDP-43) positive inclusions (FTLD-TDP), and with tau positive inclusions (FTLD-tau), account for the vast majority of cases, representing around 50% and 40% of FTLD cases, respectively[3,4].

Even though progress has been made in identifying genetic risk factors for diseases under the FTLD umbrella[5–9], the molecular mechanisms driving FTLD pathology are not completely understood. Mounting evidence reveals changes in the FTLD brain gene expression landscapes[10–14]. However, studies investigating non-sequence-based regulatory mechanisms such as epigenetic modifications in FTLD brain tissue are limited[15–18]. DNA methylation variation, the most well studied epigenetic modification, have consistently been associated

with Alzheimer's disease pathology in epigenome-wide studies (EWAS) and subsequent meta-analysis[19–21]. In FTLD, brain tissue EWAS are scarce and limited to a single PSP study[15].

To investigate further the relevance of DNA methylation variation in FTLD, we set out a study investigating epigenome-wide DNA methylation variation in frontal lobe tissue from three cohorts, spanning different subtypes of FTLD-TDP and FTLD-tau subgroups, followed by an EWAS meta-analysis, and co-methylation network analysis in each cohort, and subsequent module preservation analysis in the other datasets. Through the EWAS meta-analysis we identified four differentially methylated loci shared across FTLD subgroups and subtypes, including CpGs in *OTUD4* and *CEBPZ*. We also identified co-methylation modules associated with the FTLD status, FTLD subtypes, and pathological features (e.g. neuronal loss scores). Functional and cellular enrichment analyses have shown an overrepresentation of ontology terms related to regulation of gene expression and ubiquitin system as well as specific cell types, including pyramidal neurons and endothelial cells, across FTLD subgroups and subtypes. The meta-analysis hits in *OTUD4* and *CEBPZ* were found to be co-methylated in all three independent datasets and to be part of co-methylation modules that were strongly associated with the disease status, further supporting their role in FTLD. Our findings implicate DNA methylation in the dysregulation of important processes in FTLD, including the ubiquitin system, RNA/stress granule formation and glutamatergic synaptic signalling.

METHODS

Demographic and clinical characteristics of post-mortem brain donors

For FTLD cohort 1 (FTLD1), all post-mortem tissues originated from brains donated to the Queen Square Brain Bank archives, where tissues are stored under a licence from the Human Tissue authority (No. 12198). Both the brain donation programme and protocols have received ethical approval for donation and research by the NRES Committee London – Central. All cases were characterized by age, gender, disease history (including disease onset and duration) as well as neuropathological findings. For FTLD cohort 2 (FTLD2), all post-mortem tissues were obtained under a Material Transfer Agreement from the Netherlands

Brain Bank, and MRC King College London, as described by Menden et al[22]. For FTLD cohort 3 (FTLD3), data made available by Weber et al.[15] was retrieved from GEO (accession code GSE75704). Figure 1 shows an outline of the study design and analysis framework. More details on each cohort are presented in Table 1.

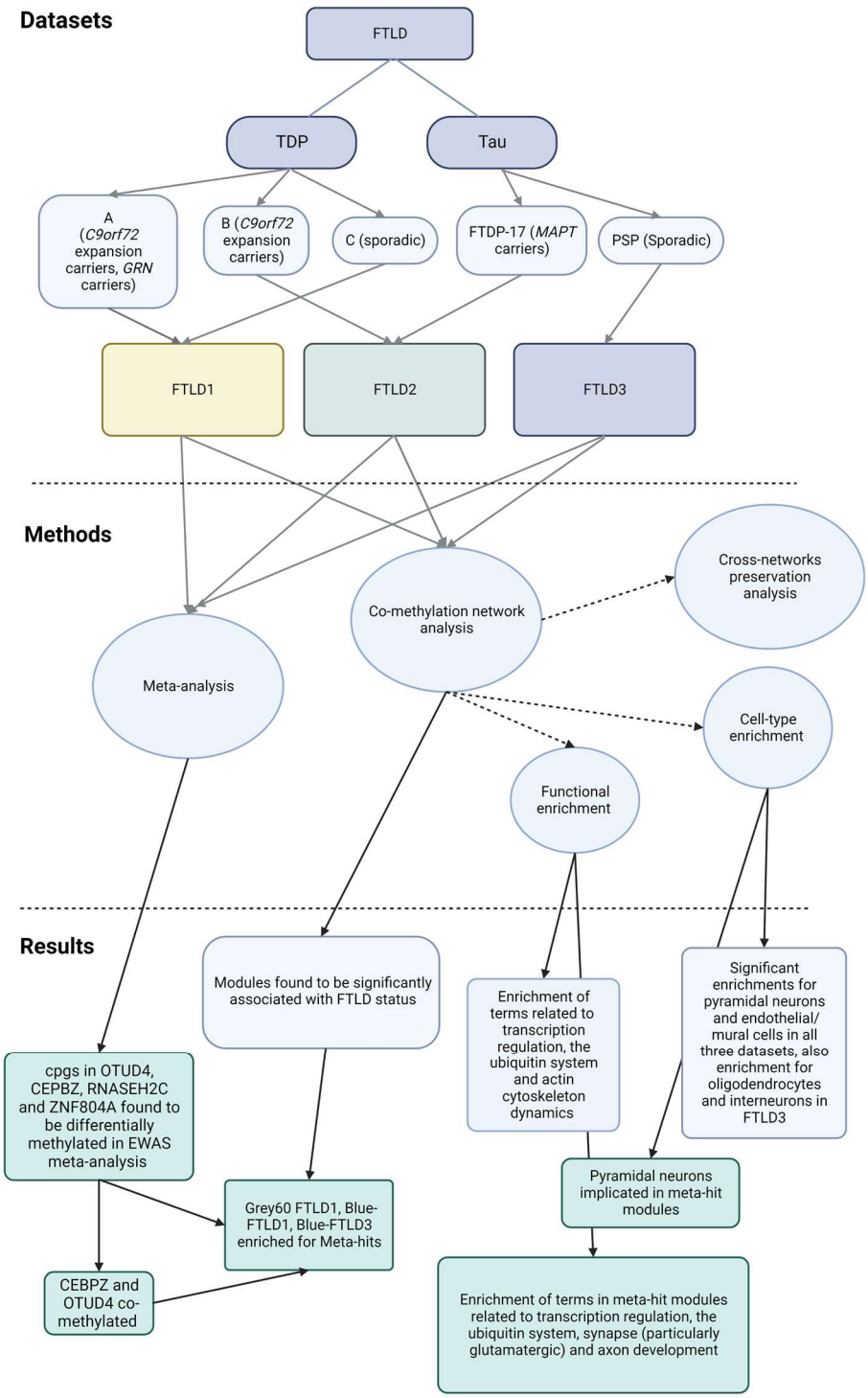

Figure 1. Outline of the study design, analysis framework and main results. FTLD – Frontotemporal lobar degeneration; PSP – Progressive supranuclear palsy. Figure created with BioRender.

Table 1: Clinical and pathological characteristics of the three FTLD cohorts and selected models for cohort-specific EWAS.

Cohort	Pathological FTLD subtypes present	Samples included after quality control + age/sex distribution	Regression models used for cohort-specific EWAS
FTLD1	FTLD-TDP type A (*C9orf72* mutation carriers), and FTLD-TDP type C (sporadic)	15 FTLD donors: mean age±SD = 70.07±5.59 years, gender= 7 males/8 females 8 neurologically normal control donors: mean age±SD = 75.75±5.63 years, gender = 3 males/5 females.	*~ 0 + disease + age + SOX10^{+} proportions + Double^{-} proportions + array* (0 surrogate variables detected)
FTLD2[22]	FTLD-TDP types A and B (*C9orf72* and *GRN* mutation carriers), and FTLD-tau (FTDP-17 - *MAPT* mutation carriers)	29 FTLD donors: mean age±SD = 62.17±7.78 years, gender=13 males/16 females 13 neurologically normal control donors : mean age±SD = 80±8.93 years, gender=5 males/8 females	*~0 + disease + age + sex + SOX10^{+} proportions + Double^{-} proportions + array + slide* (0 surrogate variables detected)
FTLD3[15]	FTLD-tau (sporadic PSP)	93 FTLD donors: mean age±SD = 71.16±5.32, gender = 54 males/39 females 70 neurologically normal control donors: mean age±SD = 76.17±7.93, gender = 45 males/25 females	*~0 + disease + age + SOX10^{+} proportions + Double^{-} proportions + array + slide + surrogate variable* (1/1 surrogate variables detected)

FTLD – Frontotemporal lobar degeneration; FTLD-TDP – FTLD with 43 kDa transactive response DNA-binding protein (TDP-43) positive inclusions; FTLD-Tau – FTLD with tau positive inclusions; FTDP-17 – frontotemporal dementia and parkinsonism linked to chromosome 17; PSP – progressive supranuclear palsy; SD – Standard deviation.

Measures of brain atrophy and neuronal cell loss and pathology related traits

For FTLD1 and a proportion of cohort FTLD2, formalin-fixed paraffin-embedded (FFPE) sections were also available for more detailed neuropathological evaluations, including sections stained for standard haematoxylin and eosin (H&E) and TDP-43 immunohistochemistry.

For FTLD1 and FTLD2, microscopic atrophy were assessed on H&E stained slides, by examining the cortical thickness and neuronal loss in the frontal and temporal cortices. A four point grading system was used in comparison to a neurological normal control with no underlying neurodegenerative changes: 0 - the cortical thickness was within normal limits and no neuronal loss was observed; 1 - reduction in cortical thickness but the number of neurons was comparable to normal levels; 2 - reduction in cortical thickness and reduction

in the numbers of neurons; 3 - severe reduction in cortical thickness and no neurons observed. For each region, the microscopic atrophy was scored semi-quantitatively by an experienced observer blinded to clinical, histopathological and genetic status, at an objective magnification of × 20. Macroscopic atrophy was also determined for FTLD1 based on observations of gyri and sulci from the coronal slices observed during brain cutting procedures. Levels of atrophy were graded, as previously described[23], into four stages: none, mild, moderate, and severe.

These neuropathological scores of the frontal and temporal regions were used in the correlations with the EWAS meta-analysis CpG hits as well as in module-trait analysis with the DNA co-methylation modules from the network analysis.

DNA methylation profiling and data quality control

For FTLD1, genomic DNA was extracted from carefully dissected flash frozen frontal cortex grey matter tissue using standard protocols. Bisulfite conversion was performed with the EZ DNA Methylation Kit (Zymo Research) using 500 ng of genomic DNA. For FTLD2 and FTLD3, DNA extractions and bisulfite conversions were performed previously as described by Menden et al.[22] and Weber et al.[15]. Genome-wide methylation profiles were generated using the Infinium HumanMethylationEPIC BeadChip (Illumina) for FTLD1 and FTLD2, or the Infinium HumanMethylation450 BeadChip (Illumina) for FTLD3, as per the manufacturer's instructions.

Beta values ranging from 0 to 1 (approximately 0% to 100% methylation, respectively), were used to estimate the methylation levels of each CpG site using the ratio of intensities between methylated and unmethylated alleles. Data analysis was conducted using several R Bioconductor packages as previously described[24]. All three cohorts were subjected to harmonized quality control checks and pre-processing. Briefly, raw data (idat files) were imported and then rigorously pre-processed and thorough quality control checks were performed with minfi[25], wateRmelon[26], and ChAMP packages[27]. The following criteria were used to exclude probes that did not pass quality control checks from further analysis: 1) poor quality, 2) cross reactive, 3) included common genetic variants, and 4) mapped to X or

Y chromosome. In addition, samples were dropped during quality control if: 1) they presented with a high failure rate (≥ 2% of probes), 2) the predicted sex did not match the phenotypic sex, and 3) they clustered inappropriately on multidimensional scaling analysis. Beta values were normalised with ChAMP using the Beta-Mixture Quantile (BMIQ) Normalisation method. M-values, computed as the logistic transformation of beta values, were used for all statistical analysis, as recommended by Du et al.[28]

As significant batch effects were detected during quality control checks, and different FTLD subgroups/subtypes were studied in FTLD1-3, the three cohorts were analysed separately first and then meta-analysed. Similarly, co-methylation network analyses were conducted on each cohort separately, and module preservations were then cross-checked with data from the other cohorts (as described in more detail below).

Cell type deconvolution based on DNA methylation data

As DNA methylation patterns are often cell-type specific, changes in different brain cell-type proportions constitute an important confounding factor for DNA methylation studies performed on 'bulk' brain tissue. We have used a novel cell-type deconvolution algorithm described by Shireby et al.[21] which brings more granularity and expands previous methods that would account only for neuronal (NeuN+) versus all other cell types (NeuN-). This new method uses novel DNA methylation reference panels data obtained from fluorescence activated sorted nuclei from cortical brain tissue to estimate the relative proportions of neurons (NeuN+), oligodendrocytes (SOX10+) and other brain cell types (Double- [NeuN-/SOX10-]). Cell-type proportions in bulk brain tissue were thus estimated using the CETYGO (CEll TYpe deconvolution GOodness) package (https://github.com/ds420/CETYGO), and the sorted cell-type reference datasets as described by Shireby et al.[21]. Pairwise comparisons between FTLD cases and controls were conducted using Wilcoxon rank sum test with Benjamini-Hochberg correction for multiple testing, and adjusted $p<0.05$ was considered significant.

Differential methylation analysis and EWAS meta-analysis

We have applied linear regression models (Table 1) using the M-values as the input to identify associations between DNA methylation variation at specific CpG sites and FTLD using the limma package[29]. For FTLD1, we have accounted for possible confounding factors, such as age as well as factors detected in principal components 1 and 2 as seen in Singular Value Decomposition (SVD) plots (ChAMP package), which included cell proportions (SOX10+ and Double-) and sample position in the array. Using this regression model, no surrogate variables were detected with the num.sv function of the SVA package[30], meaning there were no remaining unknown, unmodelled, or latent sources of noise[29]. False discovery rate (FDR) adjusted p-values <0.05 were considered genome-wide significant. The same process was applied to FTLD2 and FTLD3, cohort-specific regression models are shown in Table 1.

We used the estimated coefficients and SEs obtained from the regression models described above for the three FTLD cohorts, to undertake an inverse variance meta-analysis using the metagen function from the meta R package[31]. Only methylation probes present in all datasets (N= 363,781) were considered for this analysis, and a conservative Bonferroni significance was defined as $p < 1.374 \times 10^{-7}$ ($p < 0.05/363,781$) to account for multiple testing. We report random-effects meta-analysis results as the three cohorts included different FTLD subgroups/subtypes according to the neuropathological classification possibly leading to high heterogeneity in the meta-analysis.

Co-methylation network analysis

To identify clusters of highly correlated CpGs (co-methylation modules) in an unsupervised manner, i.e. agnostic of gene ontology, we used a systems biology approach based on weighted gene correlation network analysis (WGCNA)[32]. For this analysis, we focused on CpGs present in all three FTLD datasets, non-intergenic CpGs (i.e. CpGs that map to genes), and selected the top 20% with the highest variance across individuals regardless of their disease status in each cohort (N= 56,001 CpG sites). After outlier exclusion, 23, 42 and 162 samples remained in the FTLD1, FTLD2 and FTLD3 cohorts, respectively. For each network,

we have used the M-values adjusted as described above, and constructed signed networks. Modules were calculated using the WGCNA blockwiseModules function with a soft-thresholding power of 14, 10 and 8 for the FTLD1, FTLD2 and FTLD3 network, respectively. Module membership (MM) was then reassigned for each network using the applyKMeans function of the CoExpNets package[33]. Highly connected CpGs within a module (hub CpGs) present with high MM values to the respective module. In the results section, we refer to hub CpGs as those with the highest MM within a given module.

By using a principal component analysis on the CpG methylation values within each module, the CpGs inside each module were represented by a weighted average, the module eigengene (ME). The MEs were then correlated with the FTLD status, FTLD subtypes, and other sample traits, including disease onset and duration, measures of macroscopic and microscopic atrophy, and other pathology related traits, as available for each cohort.

To gain insights into the biology underlying FTLD-related modules, we carried out functional enrichment for CpGs mapping to genes using the default parameters of clusterProfiler[34]. We also carried out cell-type enrichment analysis on the FTLD-related modules using the package EWCE[35] and associated data[36].

DNA methylation cross-networks module preservation analysis

As a method for differential network analysis, i.e. to identify which co-methylation modules in each of the three generated FTLD networks are preserved (i.e. shared) or perturbed (i.e. unique) in the other two datasets, we employed module preservation analysis, as described by Langfelder et al.[37] . For each network (taken as the “reference dataset”), module preservation in the other two datasets (the “test data”) was calculated using the modulePreservation function implemented in WGCNA. In all instances, the “test data” contained methylation values (adjusted M-values) for the 56,001 CpG sites used to construct the “reference dataset” network. As a measurement of module preservation, we used the Z-summary statistic (a composite measure to summarise multiple preservation statistics). A Z-summary greater than 10 indicates that there is strong preservation of this

module in the “test data”, a Z-summary of between 2 and 10 indicates moderate preservation, and a Z-summary less than 2 indicates no preservation.

Comparisons of DNA methylation hits with FTLD frontal/temporal cortex gene expression data

To examine the gene expression patterns of the EWAS meta-analysis gene hits, we have used previously published transcriptomics data from bulk frontal cortex tissue of FTLD-TDP cases and controls[14] as well as bulk temporal cortex tissue of FTLD-tau cases (PSP) and controls[38]. To further infer the expression patterns of selected DNA methylation gene hits in specific brain cell types, we have also correlated gene expression levels (adjusted for age, sex, and RNA integrity number) with cellular proportions using data from Hasan et al.[14], with cellular proportions estimated using the method described by Mathys et al.[39]

Comparisons of DNA methylation hits with FTLD-TDP frontal cortex proteomics data

To examine the gene expression patterns of the EWAS meta-analysis gene hits at the protein level, we have investigated proteomics data from FTLD-TDP and controls. Briefly, frontal cortex homogenate of post-mortem human brain tissue was prepared from control (N=6), FTLD-TDP type A with *C9orf72* repeat expansion (N=6), and FTLD-TDP type C (N=6) cases. Proteins in both the soluble supernatant and the insoluble pellet fraction were analysed, and samples were pooled per disease group (three cases per pooled sample). Proteins were quantitated using 2D-LCMS and UDMSe label-free proteomics and SYNAPT G2- Si High Definition mass spectrometer operating in ion mobility mode. Data was processed using Progenesis software, as previously described[40]. A total of 6114 proteins were detected in the supernatant, and 5108 in the pellet, with an overlap in some proteins that were found both in the supernatant and pellet. Fold-changes between FTLD-TDP subtypes compared to controls were calculated. Of the EWAS meta-analysis hits, only OTUD4 (both in supernatant and in pellet) and ZNF804A (in pellet) proteins were detected.

Comparisons of DNA methylation hits with additional datasets

We further investigated the normal expression patterns of the meta-analysis gene hits both in the human and mouse brains using single nuclei RNAseq data from the Allen Brain Map (https://celltypes.brain-map.org/)[41], and data from the Allen Mouse Brain Atlas (http://mouse.brain-map.org)[42]. Given the *OTUD4*-related findings, we have investigated the list of cortical tissue OTUD4 protein interactors made available by Das et al.[43]. The RNA granule database (http://rnagranuledb.lunenfeld.ca/) collates curated literature evidence that support gene or protein association with the stress granules (SGs) and P-bodies (PBs). We have used a list of tier 1 genes from the RNA granule database version 2.0 for comparisons with the lists of genes composing the three *OTUD4* FTLD-associated co-methylation modules.

OTUD4 immunohistochemical staining

To investigate tissue expression patterns of OTUD4 protein across the human cortex, FFPE frontal cortex tissue from 7 FTLD cases (4 FTLD-TDP type A and 3 FTLD-TDP type C) and 3 controls (overlapping with FTLD1) were utilized. Briefly, eight-micrometre-thick sections were cut from the FFPE blocks were immunostained using a standard avidin-biotin-peroxidase complex method with di-aminobenzidine as the chromogen[44]. The rabbit anti-OTUD4 antibody (Atlas Antibodies HPA036623, 1:200) was used, along with heat antigen retrieval pre-treatment prior to application of the primary antibody. The samples were mounted and examined using a light microscope.

RESULTS

Cell-type deconvolution based on DNA methylation data highlights important cellular composition differences in FTLD

To estimate brain cell type proportions in our bulk frontal cortex DNA methylation datasets, we used a refined cell type deconvolution algorithm based on reference DNA methylation profiles from purified nuclei from neurons (NEUN+), oligodendrocytes (SOX10+) and other

brain cell types (Double-)[21]. This new model controls better for cellular heterogeneity in bulk cortex tissue compared to previous models, which accounted only for neuronal (NeuN+) versus all glial cells (NeuN-). Within each sample group, we observed extensive variability in cell type proportions across cell types (Fig. 2). When comparing disease cases with controls, no overall differences were overall detected in the proportions of oligodendrocytes (SOX10+) and other glial cells (Double-) after accounting for multiple testing corrections. However, with the exception of the PSP cases (FTLD3), all FTLD subgroups/subtypes showed a significant decrease in neuronal proportions compared to controls (Wilcoxon rank sum, test adjusted-p<0.05), as expected in neurodegenerative diseases. These findings highlight the importance of adjusting for cell-type proportions in bulk tissue EWAS studies. Accounting for this allowed us to identify DNA methylation changes that are relevant to the disease rather than merely reflecting changes in cell-type composition, which could be related partly to the disease pathogenesis itself and partly due to technical issues (e.g. a result of capturing different proportions of grey and white matter during tissue dissection).

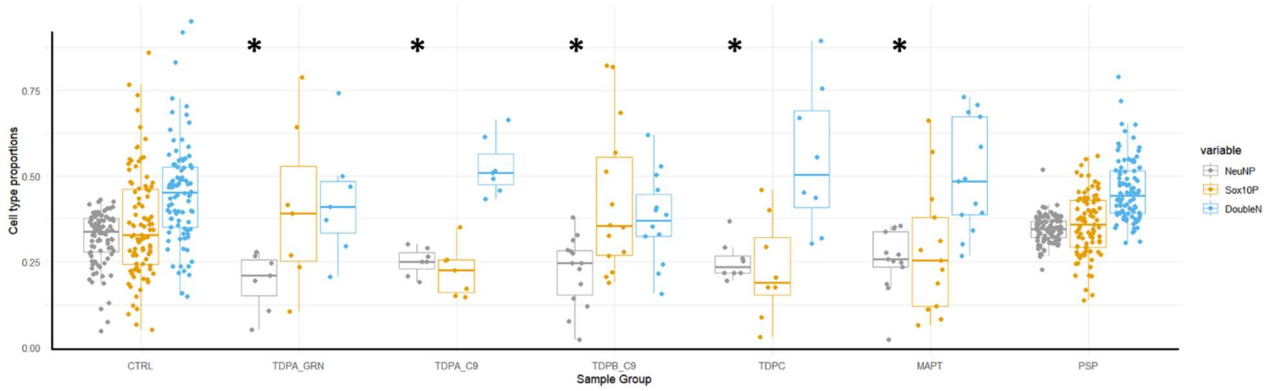

Figure 2. Brain cell-type proportion estimates derived from bulk DNA methylation data in frontal lobe of frontotemporal lobar degeneration (FTLD) and controls. *indicates significant differences when I performing pairwise comparisons between FTLD (TDP and Tau subtypes) and controls for each cell type, Wilcoxon rank sum test adjusted p<0.05. CTRL – controls; TDPA_GRN – FTLD with TDP-43 positive inclusions (FTLD-TDP) subtype A, carriers of *GRN* mutations; TDPA_C9 – FTLD-TDP subtype A, carriers of *C9orf72* repeat expansion; TDPB_C9 – FTLD-TDP subtype B, carriers of *C9orf72* repeat expansion; TDPC – FTLD-TDP subtype C, sporadic; MAPT – FTLD with tau positive inclusions (FTLD-Tau), carriers of *MAPT* mutations; PSP – FTLD-Tau, sporadic progressive supranuclear palsy (PSP); NeuNP – neuronal proportions; Sox10P – oligodendrocyte proportions; DoubleN – proportions of other brain cell types.

Frontal cortex EWAS meta-analysis identified four shared differentially methylated CpG sites across FTLD pathological subgroups and subtypes

First, we investigated DNA methylation variation in specific loci across the genome as covered by the 450K/EPIC arrays, using linear regressions models to perform cohort-specific EWAS. For FTLD1 and FTLD2, which comprise heterogeneous cases with sporadic and genetic forms of FTLD-TDP and FTLD-tau pathology, no genome-wide significant CpGs were identified. For FTLD3, which only includes cases with FTLD-tau pathology (sporadic PSP), 248 differentially methylated positions were identified (Supplementary Table S1). The top CpG cg09202319 mapped to *PFDN6* (Prefoldin Subunit 6), which is involved in promoting the assembly of cytoskeletal proteins[45]. Supplementary figure 1 shows the quantile-quantile (Q-Q) plots for each of the single cohort-specific EWAS.

Second, we meta-analysed the single cohort EWAS results, enabling an analysis of FTLD-associated differential cortical DNA methylation using tissue from 228 individuals. After Bonferroni adjustment for multiple testing ($p<1.37 \times 10^{-7}$), the meta-analysis identified four differentially methylated CpGs in FTLD compared to controls, regardless of the pathological subgroup (FTLD-TDP or FTLD-tau), and corresponding subtypes (Fig. 3, Supplementary Table S2). All those four CpGs were hypomethylated in FTLD compared to controls, and the direction of the effect was consistent across the three cohorts (Supplementary Table S2). Of note, none of these differentially methylated sites showed significant changes in previous Alzheimer's disease EWAS meta-analyses (Supplementary Table S2).

Methylation levels of both cg21028777 in *OTUD4* and cg07695590 in *CEBPZ* were negatively correlated with brain macroscopic atrophy scores and/or the severity of neuronal loss in both FTLD1 and FTLD2 (Fig. 3C-D). As these CpGs presented with lower methylation levels in FTLD compared to controls, and moreover, as decreases in methylation levels were associated with increased brain atrophy and/or neuronal loss, our findings suggest the relevance of these methylation sites in FTLD disease severity and progression. On the other hand, DNA methylation levels of cg23241637 in *ZNF804A* were positively correlated with brain macroscopic atrophy scores and the severity of neuronal loss in FTLD1 only (Fig. 3C). However, as this finding was not replicated in FTLD2 (Fig. 3D), it should be interpreted with caution.

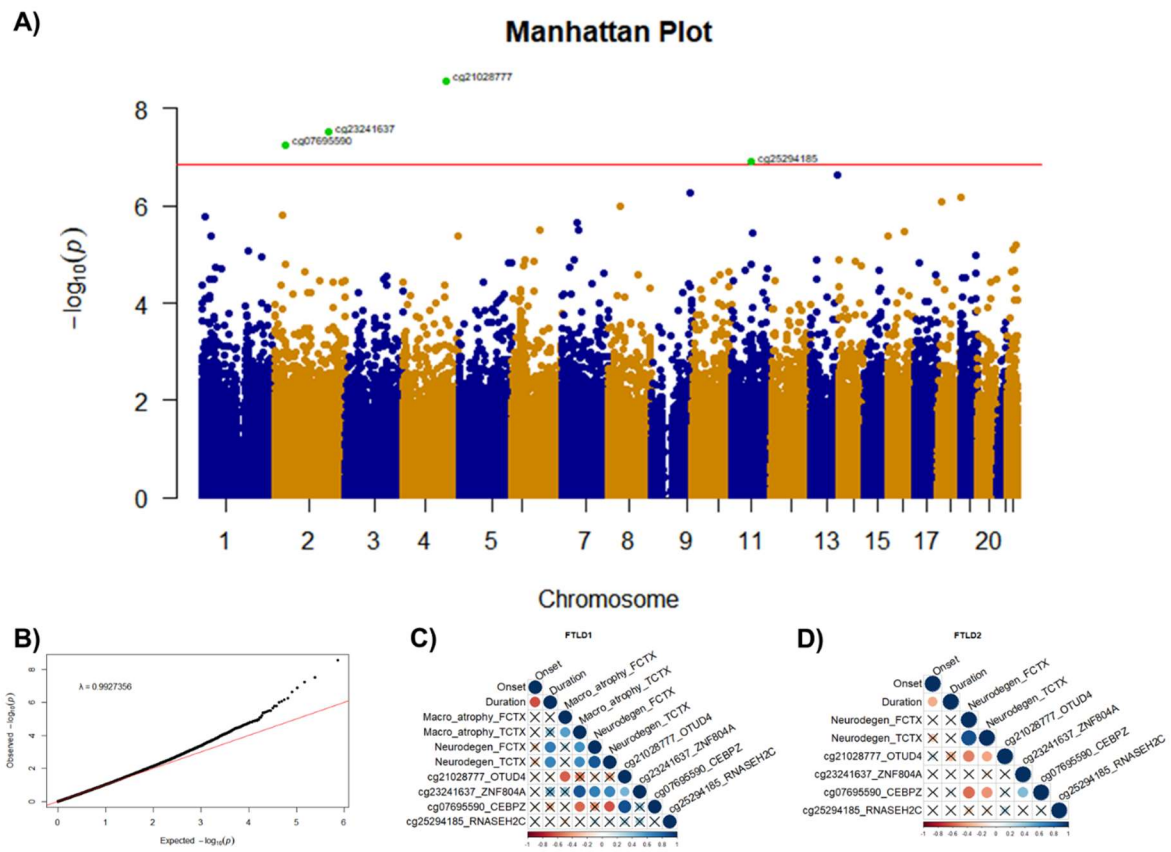

Figure 3. Results from the FTLD cross-cohort meta-analysis. A) Manhattan plot showing associations between single CpGs and FTLD from the meta-analysis random-effect results. CpGs are plotted on the x-axis according to their positions on each chromosome against association with FTLD on the y-axis (− log 10 p-value). The top line indicates genome-wide significance threshold (α) of $p = 1.37 \times 10^{-7}$. Green points indicate genome-wide significant CpGs. **B)** Quantile-quantile plot for the FTLD meta-analysis, with an estimated inflation factor of 0.99. **C-D)** Correlations between the four CpGs found to be significantly associated with FTLD in the meta-analysis and disease-related traits in two cohorts with available data, FTLD1 (**C**) and FTLD2 (**D**), blue circles indicate positive and red circles indicate negative correlations ($p<0.05$). Macro_atrophy – semiquantitative score for macroscopic atrophy; Neurodegen – semiquantitative score for severity of neuronal loss as seen in H&E staining; FCTX – frontal cortex; TCTX – temporal cortex.

Frontal cortex FTLD EWAS meta-analysis hits are consistent with downstream changes in mRNA and protein expression patterns

To investigate the downstream consequences of DNA methylation variation on gene expression in FTLD, we investigated available FTLD-TDP and FTLD-tau transcriptomic data[14,38], and FTLD-TDP proteomics data. From the EWAS meta-analysis gene hits, consistent

results were observed in both FTLD-TDP (frontal cortex) and FTLD-tau (temporal cortex) with *OTUD4*, *RNASEH2C* and *CEBPZ* showing higher expression, and *ZNF804A* showing lower expression in FTLD cases compared to controls. However, only *OTUD4* and *RNASEH2C* showed statistically significant upregulation in FTLD-TDP cases compared to controls (adjusted-$p<0.05$)[14].

Two of the four meta-analysis gene hits were detected in the frontal cortex proteomics data. OTUD4 was upregulated in FTLD-TDP in types A (supernatant fold-change = 1.63) and C (supernatant fold-change = 14.72; pellet fold-change = 6.88). On the other hand, ZNF804A was downregulated in type C (pellet fold-change = -1.36) compared to controls. These data, together with RNAseq data, support consistent dysregulation of the EWAS meta-analysis hits in FTLD, and especially *OTUD4*. Therefore, we further investigated the patterns of OTUD4 protein expression in the frontal cortex, and performed anti-OTUD4 immunohistochemical analysis (Fig. 4) in FTLD-TDP types A and C cases as well as controls that were used in the DNA methylation analysis (FTLD1 cohort). Minimal neuronal cytoplasmic staining was observed in the normal controls. However, in the FTLD-TDP cases an increase in cytoplasmic staining intensity was observed in both the grey and white matter. In the grey matter, neuronal cytoplasmic staining was seen together with nuclear glial staining. In the white matter, there was an increase in glial staining. These results are in agreement with what was observed with the proteomics and transcriptomics data.

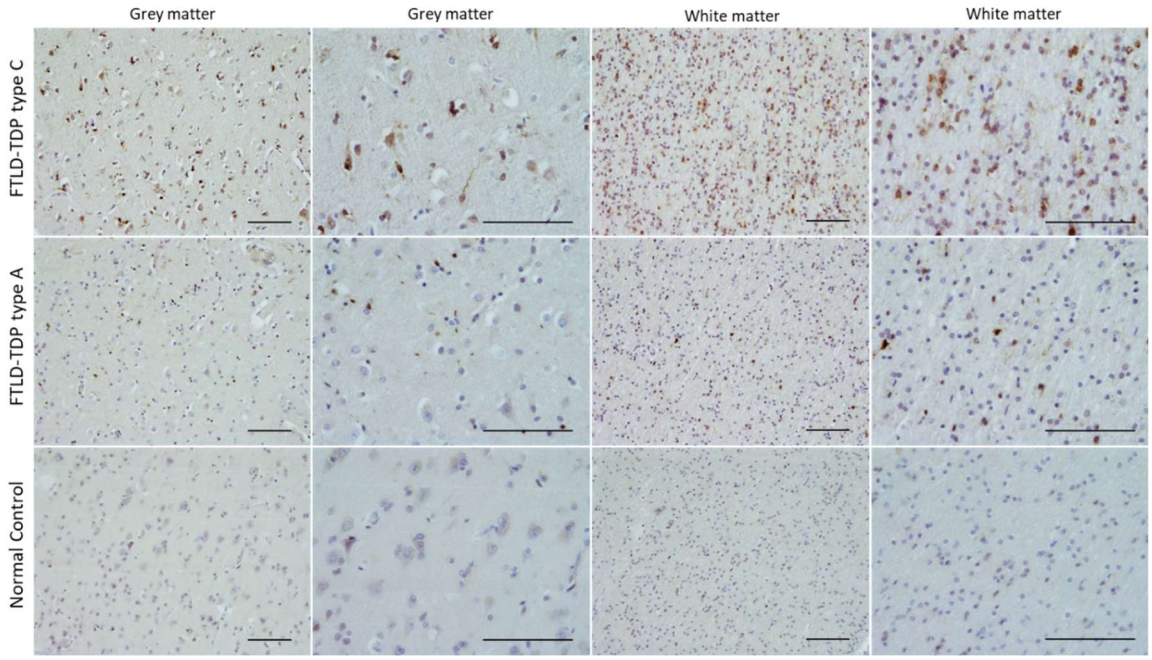

Figure 4. Immunoreactivity of OTUD4 in FTLD-TDP (N=4 type A and N=3 type C) and controls (N=3). Immunohistochemical analysis was carried in FFPE frontal cortex tissue from FTLD-TDP cases and controls overlapping with FTLD1, using a rabbit anti-OTUD4 antibody (Atlas Antibodies HPA036623, 1:200). Scale-bars represent 100 µm.

DNA co-methylation modules are associated with the FTLD status, FTLD pathological subtypes, and disease-related traits

To provide insight into higher order relationships across CpGs/genes, we have used an agnostic systems biology approach based on WGCNA and constructed co-methylation networks. Considering the top 20% most variable CpGs in each of the 3 cohorts (N = 56,001 CpGs), we have identified clusters of highly correlated CpGs, each assigned a colour name, which will be henceforth called co-methylation modules.

For the FTLD1, FTLD2 and FTLD3 networks, 9/33 ($p < 0.002$, 0.05/33 modules), 16/49 ($p < 0.001$, 0.05/49 modules) and 8/18 ($p < 0.003$, 0.05/18 modules) co-methylation modules were found to be associated with the disease status (i.e., FTLD or control), respectively (Fig. 5A-C). Our co-methylation network analysis also revealed modules associated with specific pathological subgroup/subtypes in FTLD1 and FTLD2 networks (Supplementary figure 2). In a few cases, opposite effect directions were shown in one subgroup/subtype compared to another (e.g. green and white modules in FTLD1 TDPA vs TDPC, and turquoise module in FTLD2 TDP vs Tau, Supplementary figure 2). More detailed identification of subtype-specific DNA methylation signatures warrants further investigation in future studies.

We also tested for correlations with additional disease-related traits as available for FTLD1, FTLD2, and FTLD3. We found associations between FTLD-associated DNA methylation modules and disease duration as well as with macroscopic and/or microscopic measures of atrophy/neurodegeneration in the frontal and temporal lobes (Supplementary figure 2). Four out of the 8 modules associated with the disease status in FTLD3 were also associated with tau pathological burden (Braak stage, Supplementary figure 2).

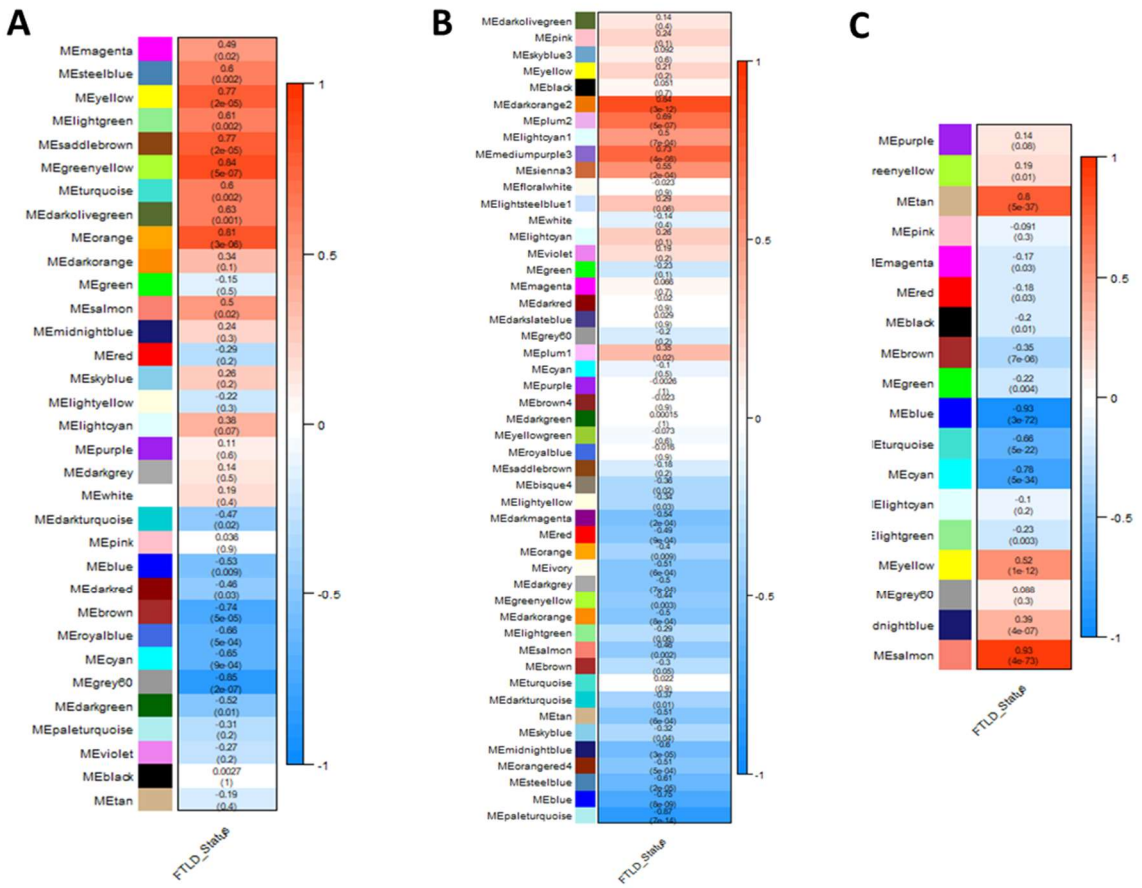

Figure 5. Module-trait correlations for the FTLD co-methylation networks. A) FTLD1; B) FTLD3; C) FTLD2. The rows represent the co-methylation module eigengenes (ME) and their colours, and the column represents the correlation of the methylation levels of CpGs in each module with disease status. P values are presented within each cell and the colour scale at the right indicates the strength of the correlation (darker cells depict stronger correlations, with blue representing negative and red representing positive correlations).

To infer which of the FTLD-associated co-methylation modules replicate across datasets, we then ran preservation analysis for each dataset against each of the networks. We found that most of the FTLD-associated co-methylation modules were indeed moderately to highly preserved (Z-summary > 2) in at least one of the other two datasets (Fig. 6), further supporting their relevance to FTLD regardless of the pathological subgroup/subtype. Exceptions to this were observed only for the FTLD1 grey60, the FTLD2 darkorange2, and the FTLD3 salmon modules, which seem to be perturbed in the other two datasets.

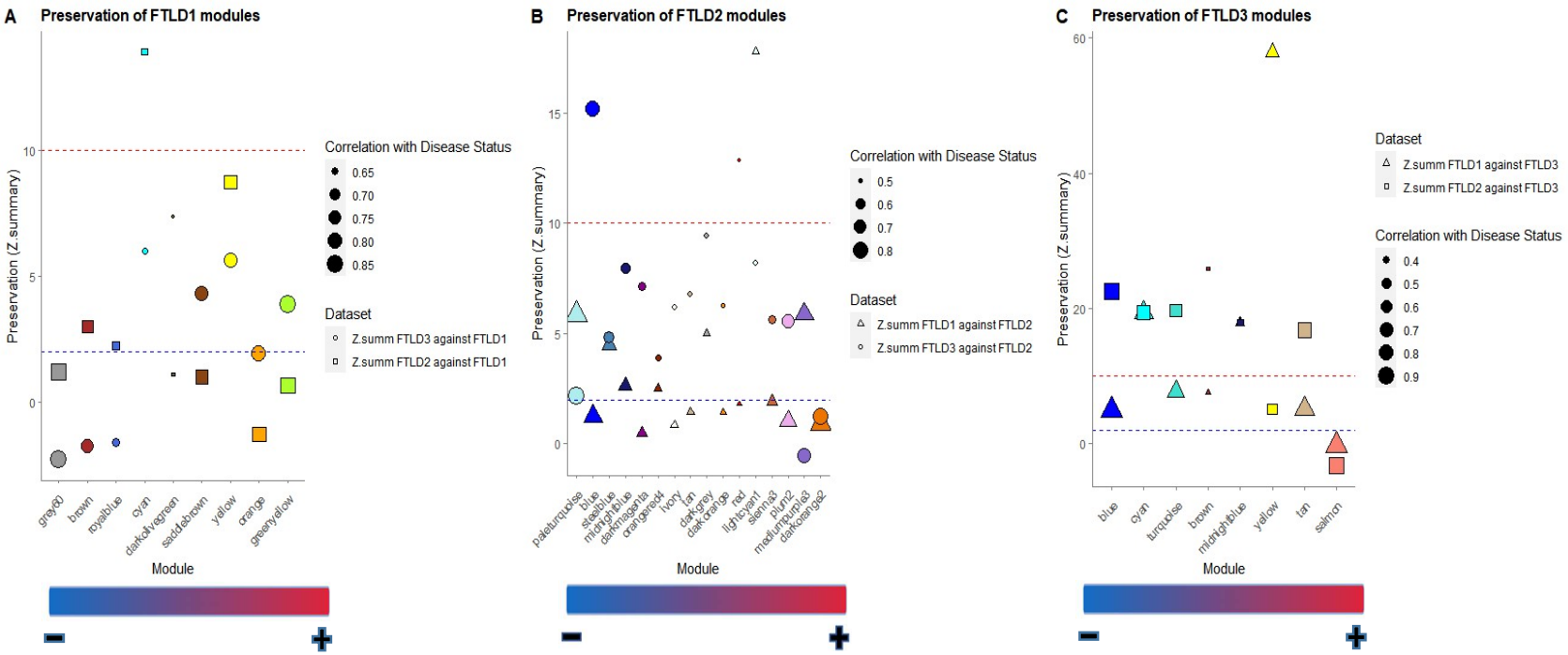

Figure 6. Preservation analysis Z-summary results for the co-methylation modules associated with FTLD in each individual network. A) Preservation of the FTLD1 network FTLD-associated modules in the FTLD2 (squares) and FTLD3 (circles) data; **B)** Preservation of the FTLD2 network FTLD-associated modules in the FTLD1 (triangles) and FTLD3 (circles) data; **C)** Preservation of the FTLD3 network FTLD-associated modules in the FTLD1 (triangles) and FTLD2 (squares) data. Colour symbols represent co-methylation modules associated with the FTLD status in the corresponding network, and the size of the symbols represents the magnitude of the association. Modules on the left hand side of the plot show the strongest negative associations with the FTLD status, while those on the right show the strongest positive associations with the FTLD status. Y-axis represents the preservation Z.summary. Modules above the red dashed line (Z.summary >10) are said to be highly preserved, modules between the blue and red dashed lines (2< Z.summary <10) are said to be moderately preserved. Modules under the blue dashed line (Z.summary <2) are not preserved.

Genes that compose FTLD-associated co-methylation modules are involved in transcription regulation, the ubiquitin system and actin cytoskeleton dynamics

We then performed functional enrichment analysis to investigate overrepresentation of shared gene ontologies across the three FTLD co-methylation networks. We found a significant enrichment for terms related with transcription regulation (e.g. DNA-binding transcription factor binding"), the ubiquitin system (e.g. "ubiquitin ligase activity"), and actin cytoskeleton dynamics (e.g. "actin binding"). This was observed across the three co-methylation networks and across different modules of each network (Fig. 7). Dysregulation of all these processes had been previously linked to FTLD[46], and our findings now support a role for DNA methylation as a mechanism involved in such dysregulation.

FTLD-associated modules depict genes relevant for pyramidal neurons and endothelial cells across all three co-methylation networks

We also aimed to elucidate whether the genes that compose FTLD-associated co-methylation modules are relevant for specific brain cell-types. Across the three networks (FTLD1, FTLD2 and FTLD3), we found significant enrichments for pyramidal neurons and endothelial/mural cells (Fig. 8), suggesting these cell types are consistently affected by the DNA methylation changes in FTLD regardless of the pathological subgroup/subtype. Previous studies with pathological assessment as well as transcriptomic analysis in FTLD brain tissue, support changes in these cell types in FTLD[14,47–50]. Additionally, in the FTLD3 network, we found signatures with overrepresentation of interneuron and oligodendrocyte makers. Of note, FTLD3 is composed of PSP cases, which, unlike the other FTLD groups studied here, is known to present with pathological accumulation of tau in oligodendrocytes[51].

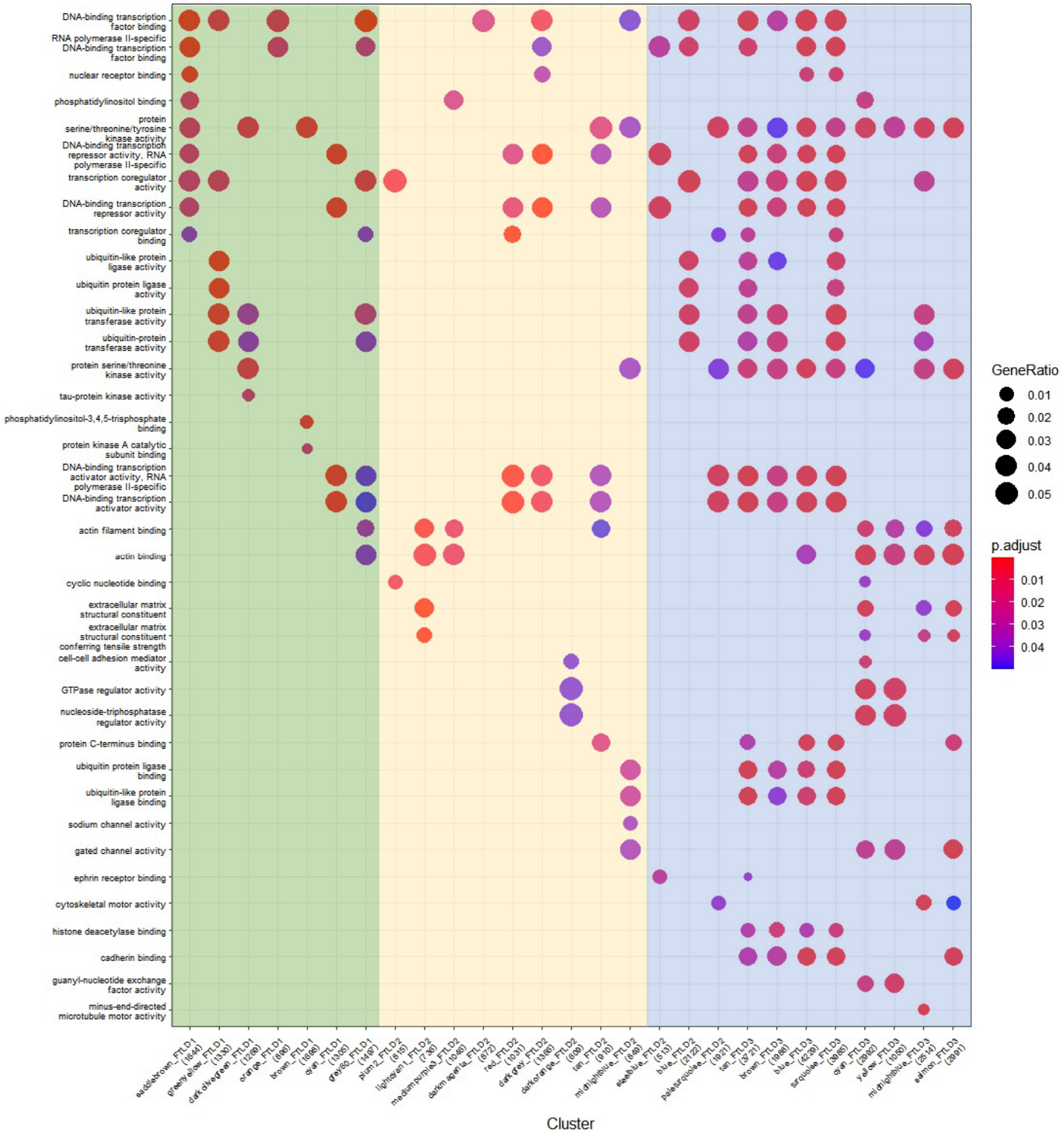

Figure 7. Functional enrichment for the FTLD-associated co-methylation modules across the three networks. Y-axis shows top enriched gene ontology terms, while x-axis depicts FTLD-associated modules in FTLD1 (green), FTLD2 (yellow) and FTLD3 (blue) co-methylation networks.

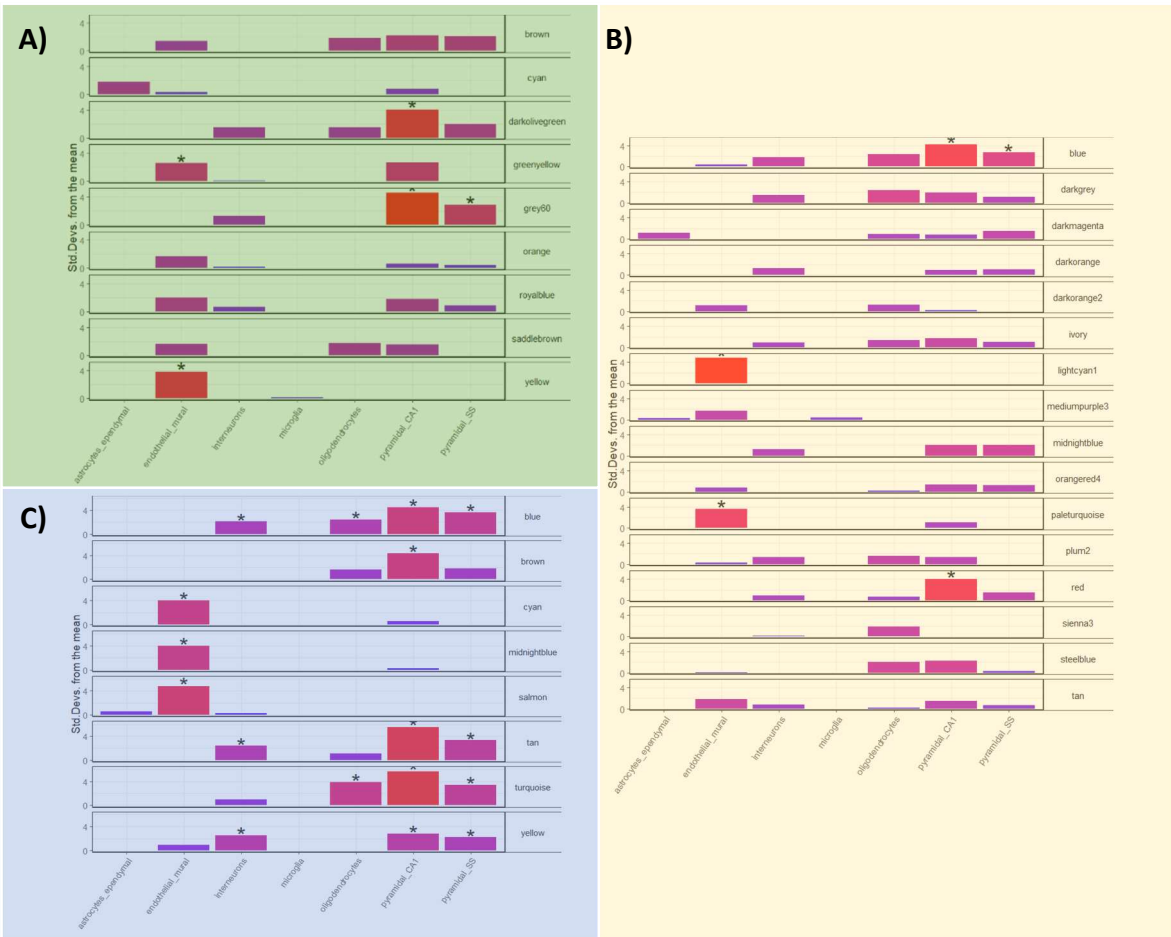

Figure 8. Cell-type enrichment for all FTLD-associated co-methylation modules. A) FTLD1 network (green); **B)** FTLD2 network (yellow); **C)** FTLD3 network (blue). Plots show enrichment of cell type markers across genes that compose FTLD-associated co-methylation signatures. For each cell type, the y-axis shows the number of standard deviations from the mean level of expression was found to be in the target gene list. Asterisks mark those cell types found to be significantly enriched with $p < 0.05$ after BH correction over all groups.

Meta-analysis hits mapping to *OTUD4* and *CEBPZ* are co-methylated in all three networks

We then examined whether the EWAS meta-analysis hits were present in the co-methylation networks and whether any co-methylation modules were enriched for those hits. All four differentially methylated CpGs identified in the EWAS meta-analysis were present in all three networks, with the exception of cg25294185 in *RNASEH2C*, which was not present in FTLD2 (Supplementary Table S3). Notably, the CpGs in *OTUD4* and *CEBPZ* were co-methylated and shared the same module in each of the three networks, grey60 in FTLD1, blue in FTLD2, and blue in FTLD3. Interestingly, these three modules show a significant enrichment for the meta-analysis hits (Fisher's exact test, odds ratios = 20.3 in

FTLD3 – blue, 26.5 in FTLD1 – grey60 and 35.4 in FTLD2 – blue, p = 0.008 for all three analysis). We therefore decided to investigate similarities across these three modules in more detail, and will henceforth be referred to as “meta-hit modules” from now on.

It is of note that only four CpGs were shared across the meta-hit modules, cg21028777 in *OTUD4*, cg07695590 in *CEBPZ*, cg05676543 in *TNIK*, and cg1639876 in *PAX1*, from which the first two correspond to meta-analysis hits (Supplementary Figure 3), highlighting their importance across the FTLD subgroups/subtypes. All three meta-hit modules were inversely related with the disease status, i.e., lower levels of methylation in CpGs composing these modules are associated with increased risk of FTLD (Fig. 5; FTLD1 grey60 r=-0.85, $p = 2x10^{-7}$; FTLD2 blue r=-0.75, $p = 8x10^{-9}$; and FTLD3 blue r=-0.93, $p = 3x10^{-72}$). FTLD2 blue was also inversely associated with the severity of neuronal loss in the frontal cortex (r=-0.48, p=0.001, Supplementary figure 2). Although not reaching statistical significance after accounting for multiple testing corrections, a similar trend was observed with the severity of neuronal loss in the temporal cortex for FTLD2 blue (r=-0.46, Supplementary figure 2) as well as for FTLD1 grey60 in both frontal and temporal cortices (r=-0.25 and r=-0.56, respectively, Supplementary figure 2). These findings further support what was observed above for the meta-analysis hits in *OTUD4* and *CEBPZ* individually (Fig. 3), and their possible relevance in disease progression/severity.

As OTUD4[43] (protein encoded by the top hit from meta-analysis) as well as tau[52] (protein accumulating in FTLD-tau), TDP-43 (protein accumulating in FTLD-TDP) and a growing number of additional FTLD-related RNA-binding proteins[53] play an important role in the biology of stress granules, we have investigated whether stress granules proteins and OTUD4 protein interactors were present in the meta-hit modules. Indeed, many genes encoding for such proteins were represented in these modules, including several genes associated with genetic FTLD risk such as *TARDBP* (encoding for TDP-43), present in FTLD1-grey60, and *FUS*, present in FTLD3-blue. The same was true for many hnRNPs (Supplementary Table S4). Probes mapping to *MAPT* (encoding for tau) were also present across the three meta-hit modules.

The meta-analysis hit gene *CEBPZ* is a transcription factor known to regulate the HSP70 promoter[54], a heat-shock protein involved in several protein folding processes. Interestingly,

the gene *HSPA1A*, which encodes for HSP70, is present in FTLD2-blue and FTLD3-blue modules together with *CEBPZ*, suggesting they are co-regulated. Additionally, hnRNPs such as *HNRNPA1*, *HNRNPC*, and *HNRNPUL1*, which are present in meta-hit modules and are also OTUD4 protein interactors, are known targets of *CEBPZ* (as described by Ma'ayan et al.[55]).

We also identified the hub genes in the three meta-hit modules (i.e., the most interconnected genes within the module). These were *HS3ST2, TLE6* and *SPRYD3* for FTLD1-grey60, FTLD2-blue and FTLD3-blue, respectively. Of note and highly relevant for FTLD, *HS3ST2* has recently been demonstrated to promote tau aggregation and to be involved in tau phosphorylation[56,57]. The importance of *TLE6* to brain related disease is supported through its association with bipolar disorder [58].

Meta-hit modules containing *OTUD4* and *CEBPZ* implicate glutamatergic synapse and pyramidal neurons

More detailed gene ontology enrichment of meta-hit modules once again highlights transcription regulation and the ubiquitin system, as well as synapse (particularly glutamatergic synapse), and axon development (Supplementary Fig. 4). All three meta-hit modules showed an enrichment for pyramidal neurons and the FTLD3 blue additionally showed an enrichment for interneurons and oligodendrocytes (Fig. 7). Further supporting the importance of *OTUD4* and *CEBPZ* in glutamatergic cells, in the normal brain (human and mouse) these genes show the highest expression in glutamatergic neurons and/or cortical and hippocampal pyramidal and granule cell layers (Supplementary Fig. 5-6).

Using gene expression data and derived cellular proportions from Hasan et al[14], we observed a positive relationship between both *OTUD4* and *CEBPZ* expression and proportions of excitatory neurons in controls and FTLD-TDP type A (Supplementary Fig. 7). This finding further supports the relevance of *OTUD4* and *CEBPZ* in excitatory glutamatergic neurons. However, that relationship is perturbed in FTLD-TDP type C (Supplementary Fig. 7), which could suggest higher expression of these genes by fewer surviving excitatory neurons and/or higher expression by other cell type(s).

DISCUSSION

We have conducted the first FTLD EWAS meta-analysis utilizing three independent cohorts and incorporating results from 228 brain donors. We identified four differentially hypomethylated CpGs shared across a range of FTLD subgroups (FTLD-TDP and FTLD-tau) and corresponding subtypes. These include CpGs mapping to *OTUD4* and *CEBPZ*, and variation in DNA methylation levels at these CpGs correlates with FTLD-pathological features. Systems biology approaches such as co-methylation network analysis are powerful methodologies for identifying pathways and networks which may be more relevant to disease pathophysiology than individual genes. We have therefore performed a co-methylation network analysis in each of the independent cohorts and identified modules associated with the FTLD disease status and FTLD-related traits. Interestingly, the meta-analysis hits in *OTUD4* and *CEBPZ* were found to be co-methylated in each of the three independent cohorts. In addition, we found co-methylation modules strongly associated with FTLD and enriched for meta-analysis hits, namely the CpGs in *OTUD4* and *CEBPZ*. Using functional and cell-type enrichment analysis of modules of interest, we identified several biological processes which have relevance to FTLD pathology, including the ubiquitin system, RNA granule formation and glutamatergic synaptic signalling, which we discuss below.

The *OTUD4* gene encodes the protein OTUD domain-containing protein 4, a de-ubiquitinating enzyme[59]. Mutations in this gene are associated with Gordon Holmes syndrome, which is characterised by ataxia and hypogonadotropism[60]. Interestingly, a combination of mutations in *OTUD4* along with mutations in *RNF216*, which codes for a ubiquitin ligase, was also found to result in dementia[60]. The protein is known to have roles in modulating inflammatory signalling[61] and in the alkylation damage response[62], and has more recently been demonstrated to interact with RNA binding proteins (RBPs), including TDP-43 (which aggregates in FTLD-TDP), which are important in the functioning of neuronal RNA granules and stress granules[63]. RNA granules are structures which facilitate the translocation and storage of mRNAs[64]. Stress granules, whilst similar, are formed when cellular stressors such as oxidative stress are present, possibly as a mechanism to reversibly block translation initiation until the stress has been removed[65,66]. Notably, similarly to TDP-43 [67], OTUD4 was shown to be important in the correct formation of stress granules[43].

Indeed, there is much evidence as to the importance of the ubiquitin system in the functioning of stress granules[68–70]. The hypomethylation of the 5'UTR region of *OTUD4* (cg21028777), which was observed as the top hit from the FTLD EWAS meta-analysis, and the inclusion of this CpG in three modules where decreased methylation was associated with increased risk of FTLD indicates that decreased methylation of this gene may be involved in the pathogenesis of FTLD. Further supporting these findings, the *OTUD4* gene and protein expression levels are dysregulated in FTLD[14,38].

Also supporting the importance of the role of ubiquitination and granule formation are the results from the functional enrichment analysis of the three network modules containing *OTUD4*, which revealed overrepresentation of terms relating to the ubiquitin system. All three meta-hit modules contained terms such as "ubiquitin protein ligase activity" and "ubiquitin-like protein transferase activity", the FTLD2-blue module also showed enrichment of the GO term "ribonucleoprotein granule", indicating that other genes in this module might also have processes relevant to granule formation, as with the meta-hit *OTUD4.* Ubiquitin signalling is well described as a process implicated in neurodegenerative disease pathology, and several genes involved in ubiquitin and ubiquitin binding processes are known to be mutated/contain risk alleles in multiple neurodegenerative diseases, including FTD[46].

Ontology terms enriched in our functional analysis of FTLD-associated modules also include many relating to regulation of transcription such as "DNA-binding transcription factor binding" and "transcription coregulator activity". Another meta-analysis CpG hit maps to the *CEBPZ* gene, which encodes the CCAAT Enhancer Binding Protein Zeta, a transcription factor implicated in cellular response to environmental stimuli through transcriptional processes that regulate heat shock factors, including HSP70[54]. HSP70 is a heat-shock protein involved in several protein folding processes, including the refolding of aggregated proteins[71–73]. Furthermore, HSP70 has been shown to have a role in the prevention of build-up of misfolded proteins in stress granules[74]. Interestingly, a CpG in *PFDN6* was the top most differentially methylated CpG in the FTLD3 (FTLD-tau) EWAS. This gene encodes for the subunit 6 of prefoldin, which is a co-chaperone of HSP70, regulates the correct folding of proteins and is involved in the proper assembly of cytoskeletal proteins[75]. Prefoldin proteins themselves have also been associated with neurodegenerative disease pathology[76,77].

Our functional enrichment analysis of the meta-hit modules, FTLD1-grey60, FTLD2-blue and FTLD3-blue, showed that these modules were enriched for GO terms (for cellular component) relating to synapses, including “asymmetric synapse”, and “postsynaptic density”, and “glutamatergic synapse”. Cell-type enrichment analysis revealed that these three modules were also significantly enriched for markers of pyramidal/glutamatergic cells. These findings were further substantiated with expression patterns of *OTUD4* and *CEBPZ* single-cell and mouse expression data. Furthermore, *TNIK*, another of the four overlapping genes in all three meta-hit modules, is implicated in the functioning of glutamatergic cells and in synaptic functioning[78–81]. Moreover, the FTLD1-grey60 hub gene *HS3ST2*, in addition to being known to have a role in tau aggregation, has also been implicated as having a role in synaptic organisation[82]. Glutamate, which is the most abundant excitatory neurotransmitter in the human brain[83], is typically associated with memory, learning and other higher cognitive functions[84], and has also been implicated in neurodegeneration[4]. The contribution of neurotransmitter deficits, and specifically, changes in glutamate and glutamate signalling have been described in FTD[8585–89]. DNA methylation has previously been suggested to be an important regulator of glutamatergic synaptic scaling (also known as homoeostatic synaptic plasticity), with demethylation found to be associated with increased glutamatergic synapse strength in cultured neurons[90], we here find evidence supporting disruption of such processes in FTLD. Homeostatic synaptic plasticity has been linked to neurodegeneration, possibly with loss of function due to pathogenesis, or through an increase as a mechanism to preserve function despite neurodegenerative deficits[91]. There is a known link between RNA granule formation and synapse plasticity; with RNA-binding protein function known to be particularly important. This has been proposed to be dysregulated in FTLD, whereby mutations in TDP-43 and FUS lead to dysregulated granule formation dynamics and consequent disturbances in mRNA translation and synaptic function[92,93]. Moreover, the levels of known OTUD4 interactor FMRP are regulated by ubiquitination in response to stimulation by the metabotropic glutamate receptor[94,95], and this is involved in the regulation of synaptic plasticity, providing another possible link between separate findings in our study.

As for any other genome-wide DNA methylation study, there are key limitations. First, by studying post-mortem tissue, i.e. the end stage of the disease, causality cannot be

elucidated. Second, because FTLD is heterogeneous, comprising several pathological subgroups and subtypes, and given the relatively small sample size per subtype, this might have hampered the identification of additional DNA methylation alterations, especially subtype-specific variation. Notwithstanding, we focused on the shared DNA methylation variation across FTLD subgroups/subtypes, and we used independent and complementary analytical approaches (EWAS followed by meta-analysis, and co-methylation network analysis followed by preservation analysis) and datasets, which identified concordant results and consistently identified the involvement of *OTUD4*, *CEBPZ* and related genes in FTLD.

In summary, this study identified genome-wide DNA methylation changes in post-mortem frontal cortex tissue of FTLD subjects, highlighting new FTLD-associated loci, and implicated DNA methylation as a mechanism involved in the dysregulation of important processes such as ubiquitin and glutamatergic signalling in FTLD. Our findings increase the understanding of the biology of FTLD and role of DNA methylation its pathophysiology, pointing towards new avenues that could be explored for therapeutic development.

Acknowledgements

The authors would also like to thank UCL Genomics centre for advice and processing of the EPIC arrays for the FTLD1 cohort. The authors would like to acknowledge the Queen Square Brain Bank (London, UK), and the Dutch Brain Bank, Netherlands Institute for Neuroscience (Amsterdam, Netherlands) for providing brain tissues from FTLD cases and controls. The Queen Square Brain Bank is supported by the Reta Lila Weston Institute of Neurological Studies, UCL Queen Square Institute of Neurology. KF is supported by the Medical Research Council (MR/N013867/1). MM is supported by a grant from the Multiple System Atrophy Trust awarded to CB. CB is supported by Alzheimer's Research UK (ARUK-RF2019B-005) and the Multiple System Atrophy Trust. JH, RH, and TR are supported by NIH NIA R56-AG055824 and U01-AG068880, and NIH NINDS U54NS123743.

References

1. Lashley, T., Rohrer, J. D., Mead, S. & Revesz, T. Review: An update on clinical, genetic and pathological aspects of frontotemporal lobar degenerations. *Neuropathol Appl Neurobiol* **41**, 858–881 (2015).
2. Cairns, N. J. *et al.* Neuropathologic diagnostic and nosologic criteria for frontotemporal lobar degeneration: Consensus of the Consortium for Frontotemporal Lobar Degeneration. *Acta Neuropathol* **114**, 5–22 (2007).
3. Goldman, J. S. *et al.* Comparison of family histories in FTLD subtypes and related tauopathies. *Neurology* **65**, 1817–1819 (2005).
4. Neumann, M. *et al.* Ubiquitinated TDP-43 in frontotemporal lobar degeneration and amyotrophic lateral sclerosis. *Science* **314**, 130–133 (2006).
5. Kouri, N. *et al.* Genome-wide association study of corticobasal degeneration identifies risk variants shared with progressive supranuclear palsy. *Nat Commun* **6**, (2015).
6. Sanchez-Contreras, M. Y. *et al.* Replication of progressive supranuclear palsy genome-wide association study identifies SLCO1A2 and DUSP10 as new susceptibility loci. *Mol Neurodegener* **13**, 1–10 (2018).
7. Chen, J. A. *et al.* Joint genome-wide association study of progressive supranuclear palsy identifies novel susceptibility loci and genetic correlation to neurodegenerative diseases. *Mol Neurodegener* **13**, 1–11 (2018).
8. Yokoyama, J. S. *et al.* Shared genetic risk between corticobasal degeneration, progressive supranuclear palsy, and frontotemporal dementia. *Acta Neuropathol* **133**, 825 (2017).
9. Ferrari, R. *et al.* Frontotemporal dementia and its subtypes: a genome-wide association study. *Lancet Neurol* **13**, 686–699 (2014).
10. Wang, X. *et al.* Alzheimer's disease and progressive supranuclear palsy share similar transcriptomic changes in distinct brain regions. *J Clin Invest* **132**, (2022).
11. Allen, M. *et al.* Divergent brain gene expression patterns associate with distinct cell-specific tau neuropathology traits in progressive supranuclear palsy. *Acta Neuropathol* **136**, 709 (2018).
12. Grundman, J., Spencer, B., Sarsoza, F. & Rissman Id, R. A. Transcriptome analyses reveal tau isoform-driven changes in transposable element and gene expression. doi:10.1371/journal.pone.0251611.
13. Brown, A. L. *et al.* TDP-43 loss and ALS-risk SNPs drive mis-splicing and depletion of UNC13A. *Nature 2022 603:7899* **603**, 131–137 (2022).
14. Hasan, R. *et al.* Transcriptomic analysis of frontotemporal lobar degeneration with TDP-43 pathology reveals cellular alterations across multiple brain regions. *Acta Neuropathol* **143**, 383–401 (2022).
15. Weber, A. *et al.* Epigenome-wide DNA methylation profiling in Progressive Supranuclear Palsy reveals major changes at DLX1. *Nat Commun* (2018) doi:10.1038/s41467-018-05325-y.
16. McMillan, C. T. *et al.* C9orf72 promoter hypermethylation is neuroprotective. *Neurology* **84**, 1622–1630 (2015).
17. Xi, Z. *et al.* The C9orf72 repeat expansion itself is methylated in ALS and FTLD patients. *Acta Neuropathol* **129**, 715–727 (2015).
18. Banzhaf-Strathmann, J. *et al.* Promoter DNA methylation regulates progranulin expression and is altered in FTLD. *Acta Neuropathol Commun* **1**, 1–15 (2013).

19. Zhang, L. *et al.* Epigenome-wide meta-analysis of DNA methylation differences in prefrontal cortex implicates the immune processes in Alzheimer's disease. *Nature Communications 2020 11:1* **11**, 1–13 (2020).
20. Smith, R. G. *et al.* A meta-analysis of epigenome-wide association studies in Alzheimer's disease highlights novel differentially methylated loci across cortex. *Nature Communications 2021 12:1* **12**, 1–13 (2021).
21. Shireby, G. *et al.* DNA methylation signatures of Alzheimer's disease neuropathology in the cortex are primarily driven by variation in non-neuronal cell-types. *Nature Communications 2022 13:1* **13**, 1–14 (2022).
22. Menden, K. *et al.* A multi-omics dataset for the analysis of Frontotemporal Dementia genetic subtypes. *bioRxiv* 2020.12.01.405894 (2022) doi:10.1101/2020.12.01.405894.
23. Schofield, E., Kersaitis, C., Shepherd, C. E., Kril, J. J. & Halliday, G. M. Severity of gliosis in Pick's disease and frontotemporal lobar degeneration: tau-positive glia differentiate these disorders. *Brain* **126**, 827–840 (2003).
24. Bettencourt, C. *et al.* White matter DNA methylation profiling reveals deregulation of HIP1, LMAN2, MOBP, and other loci in multiple system atrophy. *Acta Neuropathol* **139**, 135 (2020).
25. Aryee, M. J. *et al.* Minfi: A flexible and comprehensive Bioconductor package for the analysis of Infinium DNA methylation microarrays. *Bioinformatics* (2014) doi:10.1093/bioinformatics/btu049.
26. Schalkwyk, L. C., Pidsley, R. & Wong, C. C. Y. wateRmelon: Illumina 450 methylation array normalization and metrics. *R package version 1.2.2* Preprint at (2013).
27. Tian, Y. *et al.* ChAMP: Updated methylation analysis pipeline for Illumina BeadChips. *Bioinformatics* (2017) doi:10.1093/bioinformatics/btx513.
28. Du, P. *et al.* Comparison of Beta-value and M-value methods for quantifying methylation levels by microarray analysis. *BMC Bioinformatics* **11**, (2010).
29. Ritchie, M. E. *et al.* limma powers differential expression analyses for RNA-sequencing and microarray studies. *Nucleic Acids Res* **43**, e47–e47 (2015).
30. Leek, J. T., Johnson, W. E., Parker, H. S., Jaffe, A. E. & Storey, J. D. The SVA package for removing batch effects and other unwanted variation in high-throughput experiments. *Bioinformatics* (2012) doi:10.1093/bioinformatics/bts034.
31. Balduzzi, S., Rücker, G. & Schwarzer, G. Statistics in practice How to perform a meta-analysis with R: a practical tutorial. *Evid Based Ment Health* **22**, 153–160 (2019).
32. Langfelder, P. & Horvath, S. WGCNA: An R package for weighted correlation network analysis. *BMC Bioinformatics* (2008) doi:10.1186/1471-2105-9-559.
33. Botía, J. A. *et al.* An additional k-means clustering step improves the biological features of WGCNA gene co-expression networks. *BMC Syst Biol* (2017) doi:10.1186/s12918-017-0420-6.
34. Wu, T. *et al.* clusterProfiler 4.0: A universal enrichment tool for interpreting omics data. *The Innovation* **2**, 100141 (2021).
35. Skene, N. G. & Grant, S. G. N. Identification of vulnerable cell types in major brain disorders using single cell transcriptomes and expression weighted cell type enrichment. *Front Neurosci* **10**, 16 (2016).
36. Zeisel, A. *et al.* Cell types in the mouse cortex and hippocampus revealed by single-cell RNA-seq. *Science (1979)* **347**, 1138–1142 (2015).
37. Langfelder, P., Luo, R., Oldham, M. C. & Horvath, S. Is My Network Module Preserved and Reproducible? *PLoS Comput Biol* **7**, 1001057 (2011).

38. Wang, X. *et al.* Conserved Architecture of Brain Transcriptome Changes between Alzheimer's Disease and Progressive Supranuclear Palsy in Pathologically Affected and Unaffected Regions. *bioRxiv* 2021.01.18.426999 (2021) doi:10.1101/2021.01.18.426999.
39. Mathys, H. *et al.* Single-cell transcriptomic analysis of Alzheimer's disease. *Nature* doi:10.1038/s41586-019-1195-2.
40. Toomey, C. E. *et al.* Investigation of pathology, expression and proteomic profiles in human TREM2 variant postmortem brains with and without Alzheimer's disease. *Brain Pathol* **30**, 794–810 (2020).
41. Bakken, T. E. *et al.* Comparative cellular analysis of motor cortex in human, marmoset and mouse. *Nature 2021 598:7879* **598**, 111–119 (2021).
42. Lein, E. S. *et al.* Genome-wide atlas of gene expression in the adult mouse brain. *Nature 2006 445:7124* **445**, 168–176 (2006).
43. Das, R. *et al.* New roles for the de-ubiquitylating enzyme OTUD4 in an RNA-protein network and RNA granules. *J Cell Sci* **132**, (2019).
44. Lashley, T. *et al.* A comparative clinical, pathological, biochemical and genetic study of fused in sarcoma proteinopathies. *Brain* **134**, 2548–2564 (2011).
45. Liang, J. *et al.* The functions and mechanisms of prefoldin complex and prefoldin-subunits. *Cell Biosci* **10**, 1–15 (2020).
46. Schmidt, M. F., Gan, Z. Y., Komander, D. & Dewson, G. Ubiquitin signalling in neurodegeneration: mechanisms and therapeutic opportunities. *Cell Death & Differentiation 2021 28:2* **28**, 570–590 (2021).
47. Ferrer, I. Neurons and their dendrites in frontotemporal dementia. *Dement Geriatr Cogn Disord* **10 Suppl 1**, 55–60 (1999).
48. Gerrits, E. *et al.* Neurovascular dysfunction in GRN-associated frontotemporal dementia identified by single-nucleus RNA sequencing of human cerebral cortex. *Nature Neuroscience 2022 25:8* **25**, 1034–1048 (2022).
49. Pottier, C. *et al.* Shared brain transcriptomic signature in TDP-43 type A FTLD patients with or without GRN mutations. *Brain* **145**, 2472–2485 (2022).
50. Fyfe, I. Surprise neurovascular dysfunction in frontotemporal dementia. *Nature Reviews Neurology 2022 18:9* **18**, 509–509 (2022).
51. Williams, D. R. *et al.* Pathological tau burden and distribution distinguishes progressive supranuclear palsy-parkinsonism from Richardson's syndrome. *Brain* **130**, 1566–1576 (2007).
52. Ash, P. E. A. *et al.* TIA1 potentiates tau phase separation and promotes generation of toxic oligomeric tau. *Proc Natl Acad Sci U S A* **118**, e2014188118 (2021).
53. Baradaran-Heravi, Y., van Broeckhoven, C. & van der Zee, J. Stress granule mediated protein aggregation and underlying gene defects in the FTD-ALS spectrum. *Neurobiol Dis* **134**, (2020).
54. Lum, L. S., Sultzman, L. A., Kaufman, R. J., Linzer, D. I. & Wu, B. J. A cloned human CCAAT-box-binding factor stimulates transcription from the human hsp70 promoter. *Mol Cell Biol* **10**, 6709–6717 (1990).
55. Rouillard, A. D. *et al.* The harmonizome: a collection of processed datasets gathered to serve and mine knowledge about genes and proteins. *Database* **2016**, (2016).
56. Huynh, M. B. *et al.* HS3ST2 expression induces the cell autonomous aggregation of tau. *Scientific Reports 2022 12:1* **12**, 1–13 (2022).

57. Sepulveda-Diaz, J. E. *et al.* HS3ST2 expression is critical for the abnormal phosphorylation of tau in Alzheimer's disease-related tau pathology. *Brain* **138**, 1339 (2015).
58. Dempster, E. L. *et al.* Disease-associated epigenetic changes in monozygotic twins discordant for schizophrenia and bipolar disorder. *Hum Mol Genet* **20**, 4786–4796 (2011).
59. Mevissen, T. E. T. *et al.* OTU deubiquitinases reveal mechanisms of linkage specificity and enable ubiquitin chain restriction analysis. *Cell* **154**, 169 (2013).
60. Margolin, D. H. *et al.* Ataxia, Dementia, and Hypogonadotropism Caused by Disordered Ubiquitination. *N Engl J Med* **368**, 1992–2003 (2013).
61. Zhao, Y. *et al.* OTUD4 Is a Phospho-Activated K63 Deubiquitinase that Regulates MyD88-Dependent Signaling. *Mol Cell* **69**, 505-516.e5 (2018).
62. Zhao, Y. *et al.* Noncanonical regulation of alkylation damage resistance by the OTUD4 deubiquitinase. *EMBO J* **34**, 1687–1703 (2015).
63. Campos-Melo, D., Hawley, Z. C. E., Droppelmann, C. A. & Strong, M. J. The Integral Role of RNA in Stress Granule Formation and Function. *Front Cell Dev Biol* **9**, 808 (2021).
64. Krichevsky, A. M. & Kosik, K. S. Neuronal RNA granules: A link between RNA localization and stimulation-dependent translation. *Neuron* **32**, 683–696 (2001).
65. Buchan, J. R. & Parker, R. Eukaryotic stress granules: the ins and outs of translation. *Mol Cell* **36**, 932–941 (2009).
66. Krause, L. J., Herrera, M. G. & Winklhofer, K. F. The Role of Ubiquitin in Regulating Stress Granule Dynamics. *Front Physiol* **0**, 1043 (2022).
67. Aulas, A., Stabile, S. & vande Velde, C. Endogenous TDP-43, but not FUS, contributes to stress granule assembly via G3BP. *Mol Neurodegener* **7**, (2012).
68. Krause, L. J., Herrera, M. G. & Winklhofer, K. F. The Role of Ubiquitin in Regulating Stress Granule Dynamics. *Front Physiol* **13**, 1043 (2022).
69. Tolay, N. & Buchberger, A. Role of the Ubiquitin System in Stress Granule Metabolism. *International Journal of Molecular Sciences 2022, Vol. 23, Page 3624* **23**, 3624 (2022).
70. Müller, S. Managing stress granule disassembly with ubiquitin and its cousin. *Signal Transduction and Targeted Therapy 2021 6:1* **6**, 1–2 (2021).
71. Pemberton, S. *et al.* Hsc70 protein interaction with soluble and fibrillar alpha-synuclein. *J Biol Chem* **286**, 34690–34699 (2011).
72. Luk, K. C., Mills, I. P., Trojanowski, J. Q. & Lee, V. M. Y. Interactions between Hsp70 and the hydrophobic core of alpha-synuclein inhibit fibril assembly. *Biochemistry* **47**, 12614–12625 (2008).
73. Huang, C. *et al.* Heat shock protein 70 inhibits alpha-synuclein fibril formation via interactions with diverse intermediates. *J Mol Biol* **364**, 323–336 (2006).
74. Mateju, D. *et al.* An aberrant phase transition of stress granules triggered by misfolded protein and prevented by chaperone function. *EMBO J* **36**, 1669–1687 (2017).
75. Liang, J. *et al.* The functions and mechanisms of prefoldin complex and prefoldin-subunits. *Cell Biosci* **10**, 1–15 (2020).
76. Sörgjerd, K. M. *et al.* Human prefoldin inhibits amyloid-β (Aβ) fibrillation and contributes to formation of nontoxic Aβ aggregates. *Biochemistry* **52**, 3532–3542 (2013).

77. Liang, J. *et al.* The functions and mechanisms of prefoldin complex and prefoldin-subunits. *Cell Biosci* **10**, 1–15 (2020).
78. Wang, Q. *et al.* The psychiatric disease risk factors DISC1 and TNIK interact to regulate synapse composition and function. *Mol Psychiatry* **16**, 1006 (2011).
79. Hussain, N. K., Hsin, H., Huganir, R. L. & Sheng, M. MINK and TNIK Differentially Act on Rap2-Mediated Signal Transduction to Regulate Neuronal Structure and AMPA Receptor Function. *The Journal of Neuroscience* **30**, 14786 (2010).
80. Burette, A. C. *et al.* Organization of TNIK in dendritic spines. *J Comp Neurol* **523**, 1913 (2015).
81. Coba, M. P. *et al.* TNiK Is Required for Postsynaptic and Nuclear Signaling Pathways and Cognitive Function. *The Journal of Neuroscience* **32**, 13987 (2012).
82. Maïza, A. *et al.* 3-O-sulfated heparan sulfate interactors target synaptic adhesion molecules from neonatal mouse brain and inhibit neural activity and synaptogenesis in vitro. *Scientific Reports 2020 10:1* **10**, 1–13 (2020).
83. Zhou, Y. & Danbolt, • N C. Glutamate as a neurotransmitter in the healthy brain. doi:10.1007/s00702-014-1180-8.
84. Bliss, T. V. P. & Collingridge, G. L. *A synaptic model of memory: long-term potentiation in the hippocampus*. (1993).
85. Murley, A. G. & Rowe, J. B. Neurotransmitter deficits from frontotemporal lobar degeneration. *Brain* **141**, 1263–1285 (2018).
86. Haapasalo, A. *et al.* Toward a Glutamate Hypothesis of Frontotemporal Dementia. (2019) doi:10.3389/fnins.2019.00304.
87. Aldana, B. I. *et al.* Glutamate-glutamine homeostasis is perturbed in neurons and astrocytes derived from patient iPSC models of frontotemporal dementia. *Mol Brain* **13**, 1–17 (2020).
88. Huber, N. *et al.* Deficient neurotransmitter systems and synaptic function in frontotemporal lobar degeneration—Insights into disease mechanisms and current therapeutic approaches. *Molecular Psychiatry 2021 27:3* **27**, 1300–1309 (2021).
89. Bowles, K. R. *et al.* Glutamatergic dysfunction precedes neuron loss in cerebral organoids with MAPT mutation. *bioRxiv* 2021.02.03.429623 (2021) doi:10.1101/2021.02.03.429623.
90. Meadows, J. P. *et al.* DNA methylation regulates neuronal glutamatergic synaptic scaling. *Sci Signal* **8**, ra61 (2015).
91. de Pasquale, R., Pignatelli, M., Parsons, M. P., Jeans, A. F. & Taylor, H. B. C. Friend or Foe? The Varied Faces of Homeostatic Synaptic Plasticity in Neurodegenerative Disease. (2021) doi:10.3389/fncel.2021.782768.
92. Sephton, C. F. & Yu, G. The function of RNA-binding proteins at the synapse: implications for neurodegeneration. *Cellular and Molecular Life Sciences* **72**, 3621 (2015).
93. Ling, S.-C. Synaptic Paths to Neurodegeneration: The Emerging Role of TDP-43 and FUS in Synaptic Functions. (2018) doi:10.1155/2018/8413496.
94. Hou, L. *et al.* Dynamic translational and proteasomal regulation of fragile X mental retardation protein controls mGluR-dependent long-term depression. *Neuron* **51**, 441–454 (2006).
95. Nalavadi, V. C., Muddashetty, R. S., Gross, C. & Bassell, G. J. Dephosphorylation-induced ubiquitination and degradation of FMRP in dendrites: a role in immediate early mGluR-stimulated translation. *J Neurosci* **32**, 2582–2587 (2012).